

## A TIDALLY-STRIPPED STELLAR COMPONENT OF THE MAGELLANIC BRIDGE

DAVID L. NIDEVER<sup>1,2</sup>, ANTONELA MONACHESI<sup>1</sup>, ERIC F. BELL<sup>1</sup>, STEVEN R. MAJEWSKI<sup>2</sup>,  
RICARDO R. MUÑOZ<sup>3</sup>, RACHAEL L. BEATON<sup>2</sup>

*Draft version September 14, 2021*

### ABSTRACT

Deep photometry of the Small Magellanic Cloud (SMC) stellar periphery ( $R=4^\circ$ , 4.2 kpc) is used to study its line-of-sight depth with red clump (RC) stars. The RC luminosity function is affected little by young ( $\lesssim 1$  Gyr) blue-loop stars in these regions because their main-sequence counterparts are not observed in the color magnitude diagrams. The SMC's eastern side is found to have a large line-of-sight depth ( $\sim 23$  kpc) while the western side has a much shallower depth ( $\sim 10$  kpc), consistent with previous photographic plate photometry results. We use a model SMC RC luminosity function to deconvolve the observed RC magnitudes and construct the density function in distance for our fields. Three of the eastern fields show a distance bimodality with one component at the "systemic"  $\sim 67$  kpc SMC distance and a second component at  $\sim 55$  kpc. Our data are not reproduced well by the various extant Magellanic Cloud and Stream simulations. However, the models predict that the known HI Magellanic Bridge (stretching from the SMC eastward towards the LMC) has a decreasing distance with angle from the SMC and should be seen in both the gaseous and stellar components. From comparison with these models we conclude that the most likely explanation for our newly identified  $\sim 55$  kpc stellar structure in the eastern SMC is a stellar counterpart of the HI Magellanic Bridge that was tidally stripped from the SMC  $\sim 200$  Myr ago during a close encounter with the LMC. This discovery has important implications for microlensing surveys of the SMC.

*Subject headings:* Galaxies: interactions — Local Group — Magellanic Clouds — Galaxies: dwarf — Galaxies: individual (SMC) — Galaxies: photometry

### 1. INTRODUCTION

The Large and Small Magellanic Clouds (LMC and SMC respectively) are the two largest satellite galaxies of the Milky Way (MW) and, due to their proximity, offer the best possibility for detailed study of dwarf galaxies, especially interacting dwarf irregulars. One of the most striking features of the Magellanic system is the vast extent of its HI component – including the  $200^\circ$ -long Magellanic Stream (MS) and Leading Arm (Nidever et al. 2010) as well as the Magellanic Bridge (Muller et al. 2003). These gaseous structures are the result of past interactions of the Magellanic Clouds (MCs) with each other and the MW galaxy (Murai & Fujimoto 1980; Gardiner & Noguchi 1996; Connors et al. 2006; Růžička et al. 2010; Diaz & Bekki 2012; Besla et al. 2010, 2012, 2013). The Magellanic Bridge is widely believed to have been tidally stripped from the SMC by a recent close encounter with the LMC  $\sim 200$  Myr ago (e.g., Muller & Bekki 2007).

While the evidence of MC interactions is quite evident in HI it is less obvious in the stellar structures of the Clouds. The SMC, which is approximately ten times less massive than the LMC, is more likely to be affected by any past interactions (and is the source of much of the MS HI material in many models), and, therefore, may be the most obvious place to search for *stellar* signs of tidal disturbances.

Two decades ago, a series of papers analyzing photographic plate photometry (Hatzidimitriou et al. 1989) reached to just below the SMC horizontal branch (HB) performed the first detailed study of the SMC stellar periphery. Using red clump (RC) stars as standard candles in two fields, Hatzidimitriou & Hawkins (1989) found the line-of-sight depth to be much larger in the northeast than in the southwest. Follow-up spectroscopy showed a correlation between distance and radial velocity (RV) in the northeast RC stars (Hatzidimitriou et al. 1993) similar to that seen by Mathewson et al. (1986) in Cepheid variables closer to the center. Gardiner & Hatzidimitriou (1992) used the photographic plate photometry of all their SMC fields to trace HB stars to  $R \sim 5^\circ$  in all directions, uncovering a fairly symmetric structure but with a quick decline in density towards the west. In contrast, the young main-sequence stars have a much more irregular shape extending towards the LMC into the Magellanic Bridge region (see black contours in Fig. 1). Gardiner & Hawkins (1991) found that the change of line-of-sight depth with radius in the western SMC, increasing with radius, was more consistent with a spheroidal than disk-like structure. The notion of the stellar SMC having a spheroidal structure is argued by Zaritsky et al. (2000) and supported by a recent spectroscopic study of  $\sim 2000$  red giant branch (RGB) stars in the central  $4 \text{ kpc} \times 2 \text{ kpc}$  of the SMC that found no sign of rotation (Harris & Zaritsky 2006). In contrast, rotation is observed in the HI component of the SMC (Stanimirović et al. 2004). Many of the structural and kinematical features of the SMC are reproduced by the LMC-SMC-MW interaction simulations of Bekki & Chiba (2009) by using a spheroidal stellar distribution and extended gaseous disk.

<sup>1</sup>Dept. of Astronomy, University of Michigan, Ann Arbor, MI, 48104, USA (dnidever@umich.edu)

<sup>2</sup>Dept. of Astronomy, University of Virginia, Charlottesville, VA, 22904-4325, USA

<sup>3</sup>Departamento de Astronomía, Universidad de Chile, Casilla 36-D, Santiago, Chile (rmunoz@das.uchile.cl)

More recent work on the SMC periphery has shown it to extend much further than previously thought. Noël & Gallart (2007) detected intermediate-age and old stars in deep photometric data at  $\sim 6^\circ$  south of the SMC center, while De Propriis et al. (2010) found spectroscopically-confirmed RGB stars out to  $R \sim 6^\circ$  in the eastern SMC. Nidever et al. (2011) used photometrically-selected RGB stars to trace the structure of the SMC periphery to  $R \sim 11^\circ$  (in multiple directions) and showed that the SMC has a fairly azimuthally-symmetric structure. Nidever et al. also found that the center of the outer SMC population ( $R > 4^\circ$ ) is offset by  $\sim 0.6^\circ$  (to the east) from the center of the inner population ( $R \lesssim 3^\circ$ ) and postulated that this is due to a perspective effect because, on average, the stars to the eastern side are closer than the stars on the western side. In addition, Bagheri et al. (2013) used 2MASS and WISE catalogs to find evidence for some candidate older stars in the region between the Magellanic Clouds, while Noël et al. (2013) used deep photometry to find intermediate-age stars in a field at  $\sim 7^\circ$  from the SMC in the Magellanic Bridge.

Variable stars and stars clusters have been widely used to study the 3D structure of the inner SMC. Several studies in the 1980s found a large line-of-sight depth in the central SMC using young Cepheids (Mathewson et al. 1986, 1988), with Caldwell & Coulson (1986) finding hints of two arms in the southwest. Haschke et al. (2012) used multi-epoch OGLE-III (Udalski et al. 2008) photometry to study the 3D distribution of cepheids ( $\sim 30$ – $300$  Myr old) and RR Lyrae ( $\gtrsim 10$  Gyr old) stars in the inner SMC ( $R < 2^\circ$ ). While both populations are found to have an extended scale height, the older stars have a fairly homogeneous distribution whereas the young stars are in an inclined orientation that is closer in the northeast than in the southwest. Finally, Crowl et al. (2001) used populous SMC clusters to study the line-of-sight depth in the inner SMC ( $R \lesssim 3$  kpc) and found a  $\pm 1 \sigma$  depth between  $\sim 6$  and  $\sim 12$  kpc.

Even with all of these studies, the detailed 3D structure of the SMC stellar periphery is still not well understood in large part due to the lack of high-quality, wide-area CCD photometry in this region of the southern sky. This is unfortunate because this knowledge would enable us not only to produce a better 3D map of the SMC but also provide us with observational data of *collisionless* particles that would much better constrain the recent ( $\sim 200$  Myr) close encounter of the MCs with each other. It is thought that during that encounter the SMC might have passed right through the LMC disk (Besla et al. 2012) and produced the HI Magellanic Bridge.

In this paper we use deep Washington  $M$  and  $T_2$  photometry from the MAgellanic Periphery Survey (MAPS) to study the line-of-sight depth of core helium-burning RC stars in the SMC periphery. We find a much larger line-of-sight depth ( $\sim 23$  kpc) in four eastern fields than in our four western fields ( $\sim 10$  kpc), and a distance bimodality in three eastern fields with a newly identified component at  $\sim 55$  kpc ( $\sim 12$  kpc closer than the component at the “systemic”,  $\sim 67$  kpc SMC distance) that is most likely an intermediate-age/old stellar counterpart of the recently tidally-stripped HI Magellanic Bridge. In Section 2 we briefly describe the observations and main features of the color magnitude diagrams (CMDs). We argue in Section 3 that the extended RC seen in many of

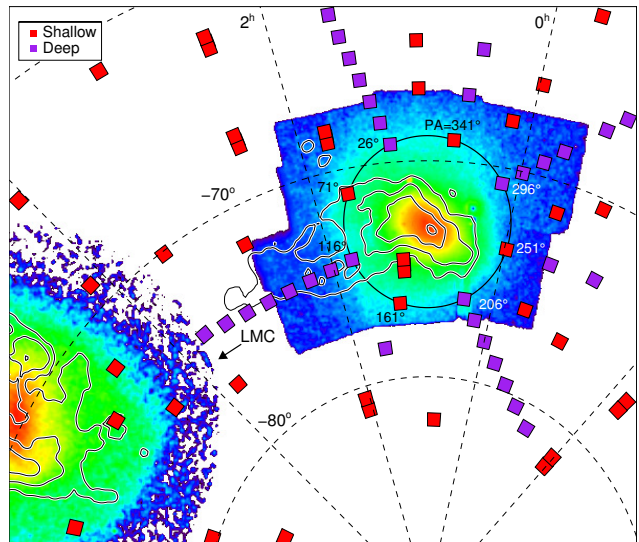


FIG. 1.— Map of the SMC showing our CTIO-4m+MOSAIC fields as filled squares (red—shallow, purple—deep). A circle at  $R_{\text{SMC}}=4^\circ$  highlights the eight fields used in our analysis. The colored image of the SMC shows the RGB starcounts using the combined Magellanic Clouds Photometric Survey (Zaritsky et al. 2002) and OGLE-III (Udalski et al. 2008) photometry (for  $R \lesssim 2^\circ$ ) and RC starcounts from the photographic plate photometry of Hatzidimitriou et al. (1989) at larger radii. The LMC is shown in RGB starcounts selected from 2MASS (Skrutskie et al. 2006). The black contours indicate the HI in the Magellanic Clouds and Bridge from Brüns et al. (2005) at levels of  $\log(N_{\text{HI}})=20.7, 21.1, 21.5$  and  $21.9$ .

our CMDs are due to large line-of-sight depths and not population effects. Density distributions as a function of distance are derived in Section 4 and compared to simulations in Section 5. Finally, a discussion of the results and their implications are presented in Section 6 and a brief summary in Section 7.

## 2. DATA

We use CTIO-4m+MOSAIC Washington  $M$  and  $T_2$  (equivalent to  $I_C$ ) photometry from the MAgellanic Periphery Survey (MAPS) for our analysis. The observations and data reduction are described in Nidever et al. (2011). Figure 1 shows the MAPS fields (filled squares) in the area of the SMC. While we have “deep” photometry (to  $M \sim 24$ ) in fields extending to  $R \approx 12^\circ$  the red clump (RC) is most prominent in our  $R=4^\circ$  fields, which are the focus of the present study.

Figure 2 shows the full  $M_0$  vs.  $(M - T_2)_0$  Hess diagrams (dereddened with the Schlegel et al. 1998 extinction maps) of four, evenly spaced in azimuth, deep fields<sup>4</sup> at  $R=4^\circ$ . The SMC RGB, RC, and main-sequence stars are clearly visible. Hess diagrams of the RC region for all eight  $R=4^\circ$  fields are shown in Figure 3. The RC morphology clearly varies substantially from field to field. The eastern fields (PA=26–161 $^\circ$ ) show a much larger RC extent in magnitude than the western fields (PA=206–341 $^\circ$ ). It was previously noted by Hatzidimitriou & Hawkins (1989) that the horizontal branch stars in the northeast of the SMC periphery have a larger line-of-sight depth (and extend to brighter magnitudes) than in the southwest.

<sup>4</sup> The field names are constructed from the field’s radius and position angle (east of north), i.e. 40S026 is  $R=4.0^\circ$  and  $\text{PA}=26^\circ$ .

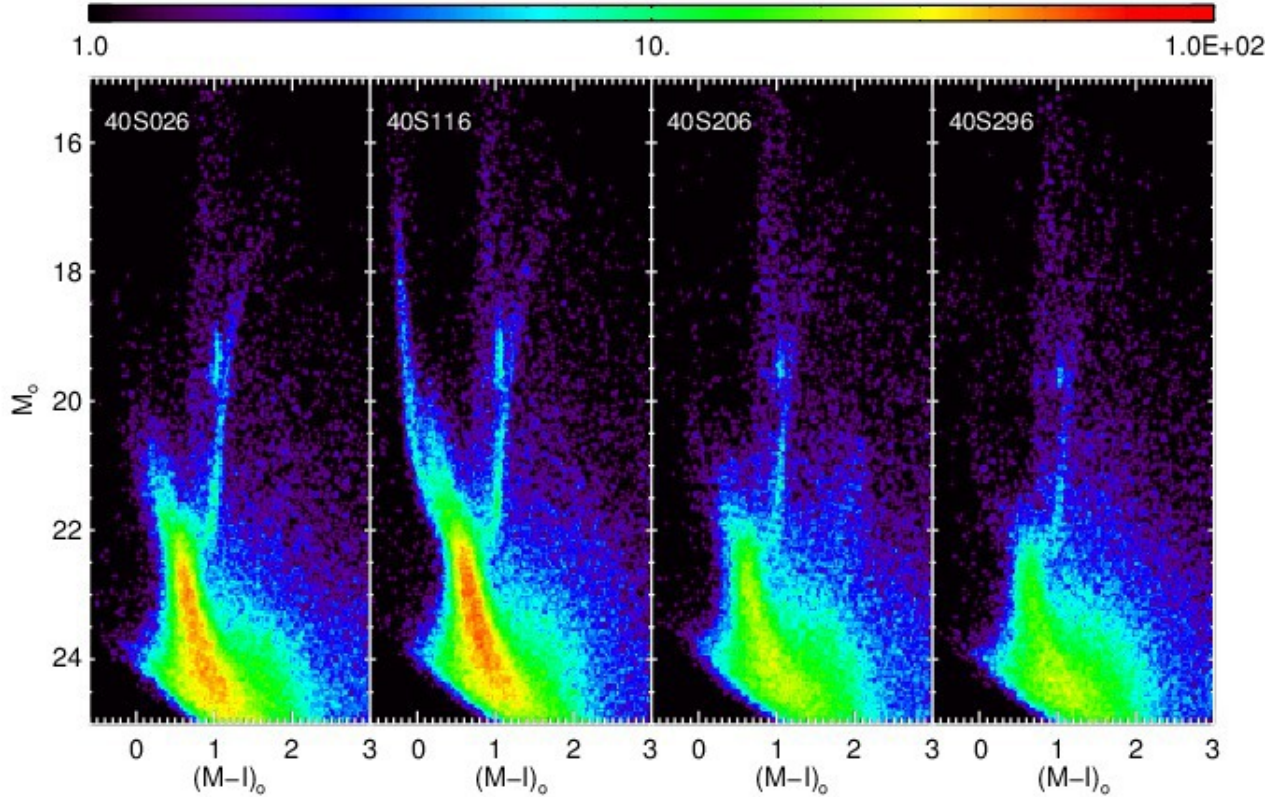


FIG. 2.— Hess diagrams for the four deepest fields at  $R=4^\circ$  showing the RGB, RC and main-sequence populations. The extended RC can be seen in the two eastern fields (40S026 and 40S116) while the two western fields display a much more compact RC. The 40S116 field is in the HI Magellanic Bridge where there is ongoing star formation and young stars extending to bright magnitudes at  $(M - T_2)_0 \sim -0.2$  can be seen.

### 3. THE NATURE OF THE EXTENDED RED CLUMP LUMINOSITY FUNCTION

An elongated distribution of the red clump (to the bright end) can be caused by reasons other than a large line-of-sight depth. The evolution of intermediate-mass He-core burning stars moves them along loops in the H-R diagram at nearly constant luminosity (“blue loop” stars). Their age at a given magnitude depends on metallicity but blue loop stars are generally quite young (a few hundred Myr to 1 Gyr; Sweigart 1987; Xu & Li 2004, and references therein) and theoretical models predict that their CMD location depends strongly on metallicity (e.g., Girardi et al. 2000). Many stars pile up on the red end of the blue loops (BL) and define a nearly vertical feature that stretches to brighter magnitudes than the RC (often spanning  $\sim 2$ -3 mag) and trending to the blue (as seen in Fig. 3 of Gallart 1998). This feature of stellar evolution can be easily confused with an extended red clump and was the primary point of contention regarding the nature of the “vertical red clump” of the LMC identified by Zaritsky & Lin (1997); these authors interpreted the feature as an intervening stellar population but this was subsequently called into question by Beaulieu & Sackett (1998). Given this precedent, we have taken steps to rule out BL stars as the cause for the extended feature observed in the CMDs of the eastern SMC fields.

We have computed a synthetic CMD that reproduces the overall features of the stellar populations of the SMC in the CMD (see Fig. 2) to compare its RC and BL distributions with the elongated feature observed at the RC

level. We have assumed a constant star formation rate (SFR) from 0.7 to 12 Gyr and metallicities of  $[\text{Fe}/\text{H}] = -1$  dex ( $[\text{Fe}/\text{H}] = -1.5$  dex) for stars younger (older) than 6 Gyr<sup>5</sup>. The model CMD was computed using the IAC-STAR code (Aparicio & Gallart 2004) adopting the BaSTI stellar library (Pietrinferni et al. 2004), a Reimers mass loss efficiency parameter value of  $\eta = 0.2$ , and a Kroupa (2002) initial mass function (IMF) from 0.1 to  $100 M_\odot$ . The magnitudes of the model CMD are expressed in the Johnson-Cousins photometric system; in particular we have chosen the bolometric correction library from Girardi et al. (2002). The magnitudes were transformed into the Washington  $M$  and  $T_2$  photometric system using the transformation equations from Majewski et al. (2000). We assumed a distance modulus of 18.9 for the SMC and did not correct the model CMD due to observational effects (incompleteness and photometric errors). Given that we expect a near 100% completeness and a  $\sim 2\%$  photometric accuracy ( $\sim 0.3\%$  internal precision) at the RC level, this correction should have little impact on the model CMD for our purposes.

Figures 4 and 5 show the observed (a) and model (b) CMDs for the 40S026 (eastern SMC) and 40S206 (western SMC) fields, respectively. The model in Figure 4b has ages ranging from 1.4 Gyr to 12 Gyr whereas the model in Figure 5b has ages ranging from 2.0 Gyr to 12

<sup>5</sup> Since these are the estimated ages and metallicities of the fields under study, as suggested in Nidever et al. (2011) by eye-fitting isochrones

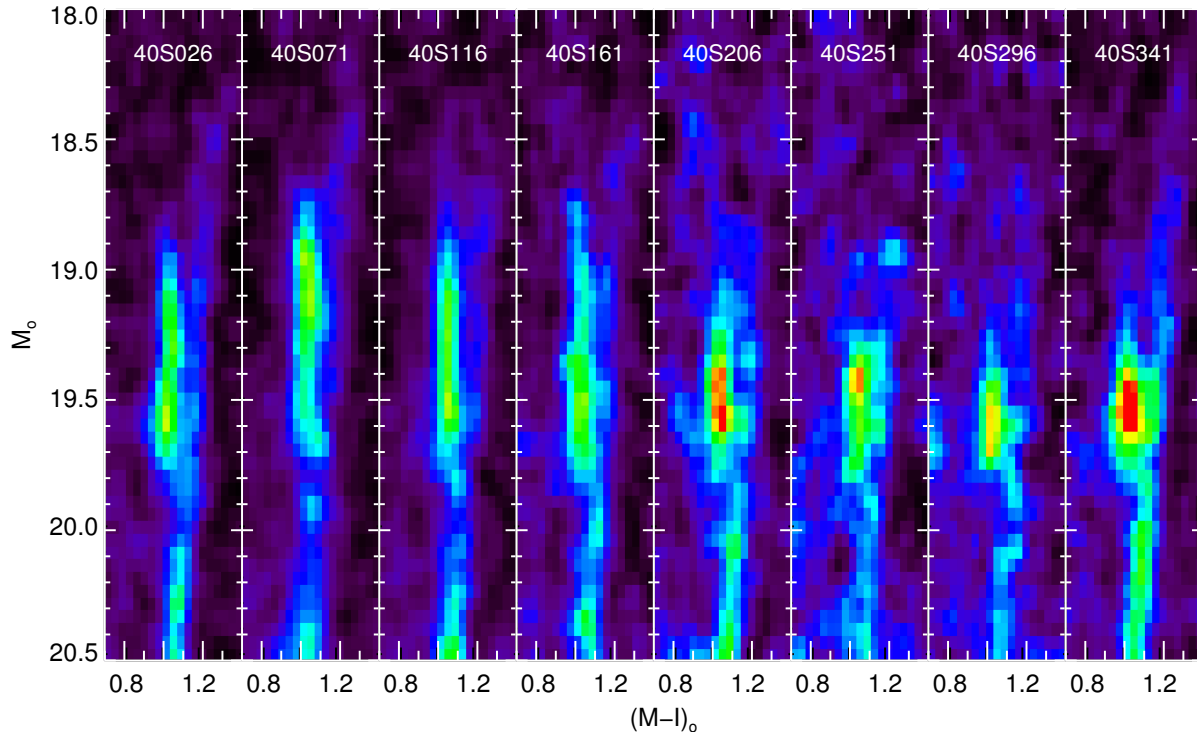


FIG. 3.— Hess diagrams of the RC region for the eight fields at  $R=4^\circ$  (arranged from left to right with increasing position angle). The Hess diagrams are scaled to the same density of SMC stars to highlight the differences in RC morphology. The four eastern fields (40S206–40S341) show an extended RC that is not seen in the western fields (40S026–40S161).

Gyr. These age ranges were chosen so that the position and characteristics of the main features (main sequence, subgiant branch, tip of the RGB) are well reproduced by the models. In Figure 4, however, there is a clear difference in the RC morphology between the model and the data. We find that the RC is much less elongated in magnitude in the model than in the CMD of the observed eastern field. This discrepancy cannot be accounted for by stellar evolutionary features such as BL stars; the model predicts that there should be almost no BL stars, given that its youngest population has an age of 1.4 Gyr. A CMD model with stars as young as 0.7 Gyr predicts more BL stars, but also shows evidence of a brighter and more populous young main-sequence, which is not seen in the data. Moreover, even if the young main-sequence from the model CMD were to agree with the data, the density of the model BL stars would still be significantly lower than that of the RC stars. Figure 6a is an attempt to reproduce the morphology of the RC region of the CMD (seen in panel b) using a spread in age and star formation rate *only* (which requires most of the young and old stars to be removed). The resulting simulated Hess diagram is *not* a good representation of the observed data, particularly on the main sequence. On the other hand, the simulated Hess diagram with a *distance* spread (convolved with the distance function for this field found in §4) in Figure 6c is a good representation. Thus, a *BL population cannot explain the elongated RC that we observe in the eastern field*. On the other hand, Figure 5 shows that the western field and model RC morphologies agree fairly well. Figures 4c and 5c show the RC luminosity function both for the data and the model. The RC stars were isolated as explained in the next section.

Note the much wider RC distribution in the eastern field when compared with the model.

#### 4. DISTANCES

To study the distance distributions, we isolate the RC stars in the CMD. Because the RC and RGB are very close in the CMD and sometimes overlap we decided to model the RGB distributions to produce a “clean” RC sample. A Hess density map of stars was created for each field in  $(M - I)_0$  and  $M_0$  in bins of 0.02 and 0.05 mag respectively. These were then smoothed with a Gaussian kernel having FWHM=2 bins. Each row, at a given magnitude, was modeled with a double-Gaussian for the RC and RGB over the magnitude range  $18.5 < M_0 < 20.5$ . After the first iteration over the magnitude range, robust linear fits with magnitude were performed to the RGB Gaussian heights, centers and widths. On the second iteration, the RGB Gaussian components were constrained to lie close to the linear fit values (especially the centers). The final RGB model was then subtracted from the density map. The final image was summed over RC colors,  $0.94 < (M - I)_0 < 1.12$ , and a similarly sized region blueward of the RC (for MW foreground) was summed and subtracted. The final RC luminosity functions are shown in Figure 7a (with Poisson errors). In some fields there is a residual RGB signal left at faint magnitudes ( $M_0 \gtrsim 20$  or RC  $d \gtrsim 80$  kpc) in the subtracted density image (which can be seen in some of the luminosity functions). However, no obvious signs of an extension of the RC are seen at these magnitudes in the CMD and so the RC luminosity functions for  $M_0 \gtrsim 20$  are ignored for the rest of the distance analysis.

Next, we use the model SMC CMD to construct an ab-

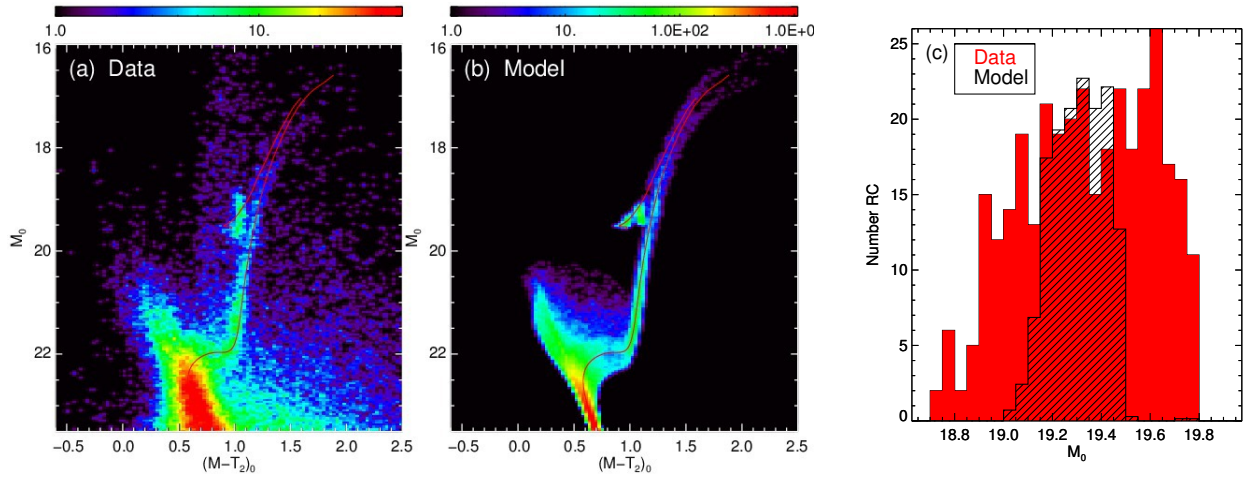


FIG. 4.— (a) Hess diagram of the 40S026 field in the eastern portion of the SMC. (b) Simulated CMD for the 40S026 field with ages of 1.4 to 12 Gyr. The red lines are  $[\text{Fe}/\text{H}]=-1.488$  age=8.0 Gyr BaSTI isochrones (Pietrinferni et al. 2004) at 60 kpc. (c) Red clump luminosity function for the data (red) and simulation (black). The observed luminosity function is much broader than the model suggesting a large line-of-sight depth.

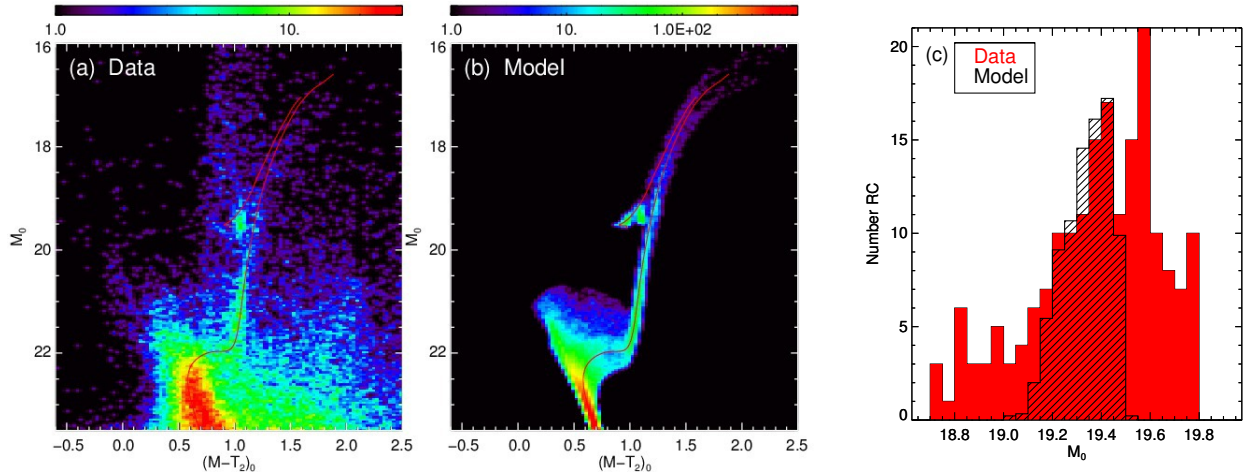


FIG. 5.— Same as Figure 4 but for the 40S206 field with model ages of 2.0 to 12 Gyr. While not as wide as the RC luminosity function of 40S026, the observed luminosity function of 40S206 is wider than the model and indicates some depth is needed to explain the observations.

solute RC luminosity function (isolating RC stars with  $1.025 < M - I < 1.12$  and  $18.7 < M < 19.8$ ) and reconstruct the density function in distance (or rather distance modulus) for each field’s observed RC luminosity function. A technique somewhat similar to the “annealing” method (which iteratively finds the state of maximum entropy) was used to derive the density function. A discrete density function in distance modulus (in 0.05 mag steps) is convolved by the absolute luminosity function (Fig. 8) to produce a model RC luminosity function that can be compared to the observed data and used to calculate  $\chi^2$  (using Poisson errors). The reconstructed density function in distance is then found by an iterative approach. The density function is initialized with the observed RC luminosity function shifted by  $-0.41$  mag (the mean SMC model RC magnitude is  $M_{\text{RC}} = +0.41$  mag). Each distance bin is then successively stepped through and its density varied until the best-fitting  $\chi^2$  value is found between the RC luminosity data and model. After stepping through all the distance bins the density

function is smoothed with a  $\text{FWHM}=1.0$  bin Gaussian kernel to smooth small-scale fluctuations. This process is then iterated many times until convergence (normally after  $\sim 10$  iterations) is achieved. To ascertain internal uncertainties in the derived density functions with distance, we performed a simple Monte Carlo simulation for each field. Poisson noise was added to the RC luminosity function and the iterative procedure performed. This was repeated 50 times and the standard deviation for each distance modulus bin (over the 50 mocks) was calculated and used as the internal uncertainty. The final density functions in distance modulus (and the uncertainties) can be seen in the right panels of Figure 7 and the best-fitting models (red) in the left panels. To estimate the depth of a field we used the span of the curve at a density level that “bisects” the distribution (i.e., half the area under the curve falls below this line and half above). The spans are shown as dotted lines in right panels of Figure 7 and the corresponding depths are indicated in the upper right-hand corner.

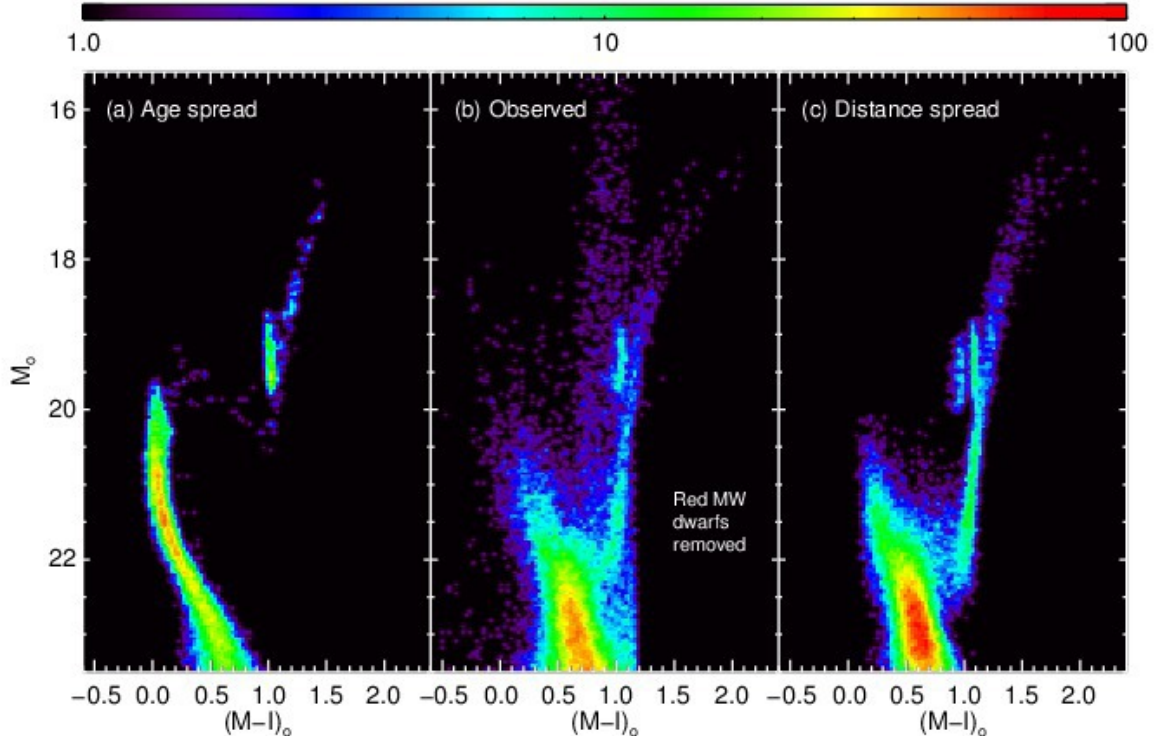


FIG. 6.— (a) A simulated Hess diagram for 40S026 using the synthetic stellar populations and *age/SFR spread only* to reproduce the morphology of the RC region (with added photometric noise using the formal observational uncertainties). To achieve this, nearly all of the young and old populations are removed to leave many stars with 0.7–1.2 Gyr. This is clearly not a good representation of the entire observed CMD. (b) Observed Hess diagram of 40S026 with red MW dwarfs removed, using the  $(M - T_2, M - \text{DDO51})_0$  diagram (Majewski et al. 2000), to reveal the structure of the upper RGB. (c) A simulated Hess diagram for 40S026 using synthetic stellar populations ( $\geq 1.4$  Gyr) convolved with a distance spread (as derived in §4 for this field) and added photometric noise (as in panel a). This is a good representation of the observed data.

The models are not perfect matches to the data and any small-scale structure in the density functions in distance should not be taken to represent real structures. However, we can use the density functions to discern broad features. The eastern fields (40S026–40S161) show large line-of-sight depths ( $\sim 23$  kpc) over a position angle range of  $135^\circ$ , while the western fields have much shallower depths of  $\sim 10$  kpc. Furthermore, three of the eastern fields (40S071, 40S116 and 40S161) show evidence for a distance bimodality (with one component at  $\sim 55$  kpc and the second at  $\sim 63$  kpc) and the fourth eastern field (40S026) has a broadened distribution, and is potentially consistent with the trend seen in the other three fields.

##### 5. COMPARISON TO MODELS

To help understand the nature of the large depth and bimodality in the eastern fields we compare our density functions to various simulations of the Magellanic Clouds and Stream: Connors et al. (2006), Diaz & Bekki (2012, hereafter DB12), and Besla et al. (2012, hereafter B12). For each simulation, particles were selected at our field locations relative to the center of the SMC in the simulation (which was sometimes shifted slightly from the observed center). There were often not enough model particles within the  $0.36 \text{ deg}^2$  area of our field sizes to make useable distance histograms. Therefore, a matching radius of  $0.5^\circ$  was used for the Connors and DB12 models, and  $0.7^\circ$  for the DB12 models. Figure 9 shows (a) our density functions, (b) the model of Connors et al. (2006), (c) the DB12 disk model, which these authors

suggest primarily represents the HI component of the SMC, (d) the DB12 spheroid1 model, which they suggest represents a spheroidal-shaped stellar component of the SMC, and (e) the B12 model1 and (f) model2 (both with stars older than 1 Gyr). It is quite immediately clear that none of the models adequately reproduce the shape and line-of-sight depth of the observed fields, although this is not entirely surprising given that these models were optimized to reproduce the gaseous Magellanic Stream. The DB12 disk model does show a bimodality in some of the eastern fields caused by the main SMC body at  $\sim 60$  kpc and the “counter-bridge” (see section 3.5 of DB12) at  $\sim 80$  kpc. In contrast, however, the two components in the data appear at  $\sim 67$  kpc (likely the main SMC body) and at  $\sim 55$  kpc (a newly-found stellar component) with very few stars beyond  $\sim 70$  kpc (except in 40S026). Therefore, it is unlikely that the observed bimodality is related to the DB12 counter-bridge (which our data effectively rule out as a stellar feature at these positions, though it could still exist at smaller radii). We note that the counter-bridge is not very prominent in the spheroid1 model (the model most likely to represent the stars) and it therefore might effectively be an HI-only feature (similar to the Magellanic Stream).

Figure 10 shows the distance– $\Delta\alpha^6$  distribution of particles near the SMC in the DB12 disk (a) and DB12 spheroid1 (b) models. Both models show extensions to

<sup>6</sup> Where  $\Delta\alpha$  is the offset (in true angle) in right ascension from the SMC center.

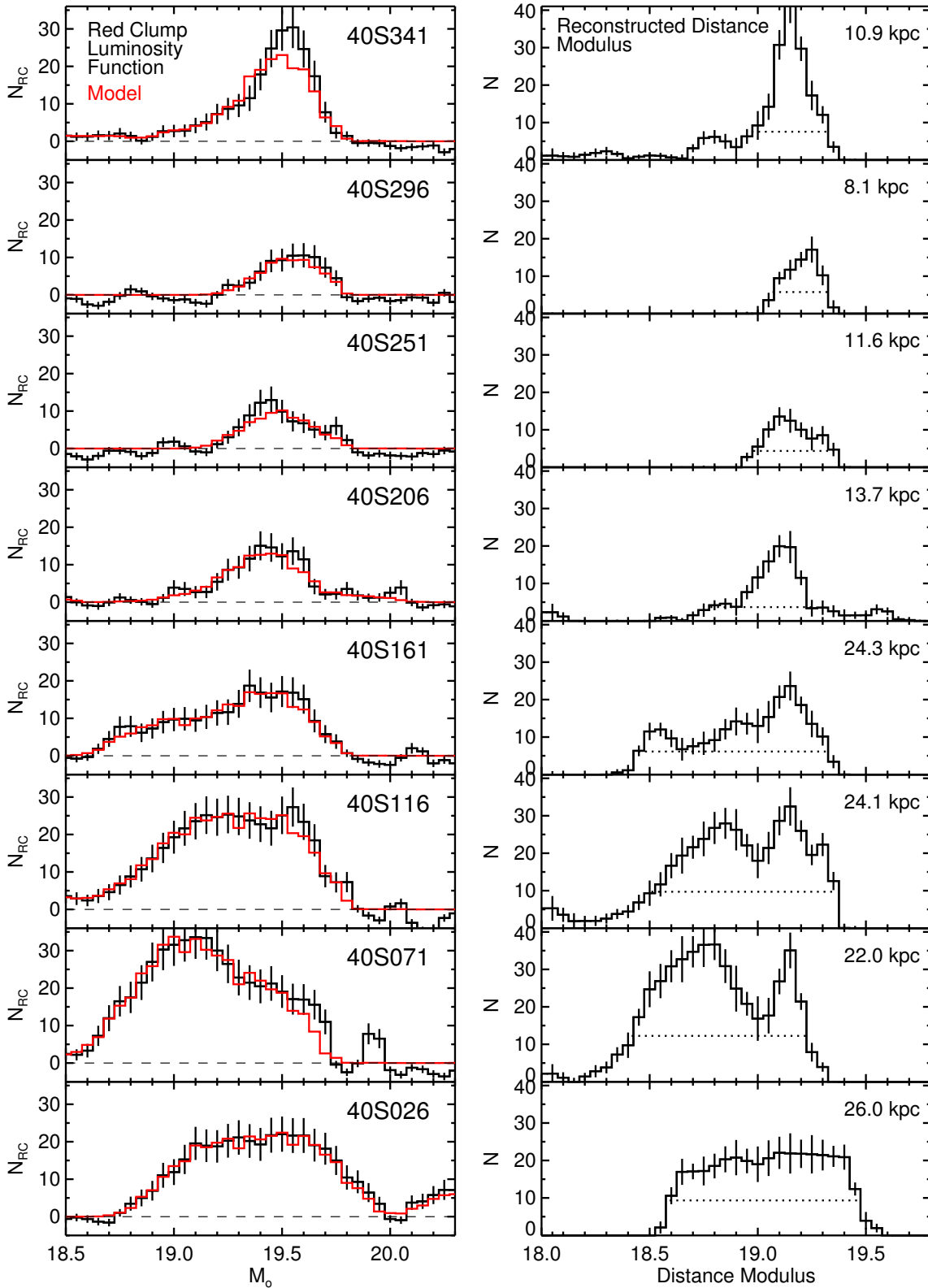


FIG. 7.— (left) Red clump luminosity functions for the eight  $R=4^\circ$  fields (with Poisson errors). Some residual RGB stars are visible at faint magnitudes in 40S026 and 40S071. The best-fitting model from the iterative procedure (see text for details) is overplotted in red. Overall the models fit well except for 40S341 which might require a narrower intrinsic RC function to fit the data. (right) Reconstructed density function with distance modulus. The errorbars show internal uncertainties found with a Monte Carlo simulation. Spans of the distribution used to calculate the depth (in upper right-hand corner) are shown as dotted lines. Three of the eastern fields (40S071–40S161) show bimodal distance distributions that have been enhanced through the reconstruction process.

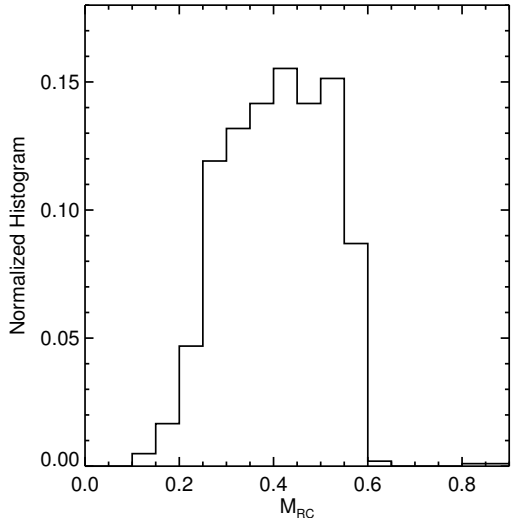


FIG. 8.— The red clump absolute magnitude luminosity function using the SMC simulated CMD. Ages from 1.4 to 12 to Gyr are included. The mean magnitude from a Gaussian fit is  $M_{RC}=+0.41$ .

the east forming the well-known structure of the Magellanic Bridge, prominently seen in HI and young stars ( $\lesssim 200$  Myr) forming in the gas. The model predictions of a significant number of particles towards the east and at closer distances, with very few to the west at those same distances, is quite similar, qualitatively, to what is seen in our stellar data. Therefore, we find that the newly-found stellar component to the eastern side of the SMC may be an intermediate-age/old ( $\sim 1$ -12 Gyr) stellar component of the tidally-stripped Magellanic Bridge (further discussed in next section).

## 6. DISCUSSION

We detect a large line-of-sight depth ( $\sim 23$  kpc) in our four eastern fields covering at least  $135^\circ$  in position angle. The western fields have a much shallower depth of  $\sim 10$  kpc with a quite sudden increase in depth between  $PA=341^\circ$  and  $26^\circ$ . Three of the eastern fields ( $PA=71^\circ$ ,  $116^\circ$ , and  $161^\circ$ ) show a distance bimodality with the farther component having  $d\sim 67$  kpc, similar to the distance of the main body of the SMC and the western fields, and the closer component at  $d\sim 55$  kpc, between the SMC and LMC distance. The fourth eastern field ( $PA=26^\circ$ ) has a large line-of-sight depth and is potentially consistent with the trend seen in the other three eastern fields. This is the first clear evidence of a distance bimodality in the eastern SMC and a newly identified structure (the component at  $\sim 55$  kpc) which we call the SMC “eastern stellar structure”.

In Section 5 we compared our data to Magellanic Clouds interaction models (Connors et al. 2006; Diaz & Bekki 2012; Besla et al. 2012, see Fig. 9). Overall the models do not match the data very well. The Connors, DB12 spheroid1 and B12 models do not show the large depth in the eastern fields that is seen in the data. In contrast, the DB12 disk model shows a large depth in some western and northwestern fields and a distance bimodality in northern and northeastern fields. The two components are from the main SMC body and the “counter-bridge”, which is a tidal stream at large distances ( $\sim 80$

kpc) and behind the SMC. While the model does have “a” bimodality, the distances do not match the data. In contrast, all of the observed fields show a component at  $d\sim 66$  kpc and the eastern fields have an extra component *in front* of the SMC at  $d\sim 55$  kpc, with almost no stars beyond 70 kpc. Therefore, there is no sign of the counter-bridge in our stellar sample. However, the DB12 disk model does show a small number of particles between  $\sim 50$ -60 kpc in the northeastern and eastern fields that are not seen in the other fields. In fact, when all particles with  $d<55$  kpc are selected they cover a wide region in the eastern SMC spanning  $PA\approx 321$ - $144^\circ$  (range of  $183^\circ$ ). The DB12 spheroid1 model shows a similar pattern of particles at this distance but at lower density and spanning a smaller position angle range of  $121^\circ$  ( $PA\approx 65$ - $186^\circ$ ). It is possible that this is the feature that we are detecting, although at a higher density than predicted by the models. At larger radii this model feature extends to even smaller distances and towards the LMC (see Fig. 10). For the DB12 disk model, which is supposed to represent the gaseous component of the SMC, this arm should represent the well-known HI Magellanic Bridge. If our new component at  $R=4^\circ$  and  $d\sim 55$  kpc is related to this feature then we very well might be seeing, for the first time, a stellar component of the Magellanic Bridge.

Even though the proximity of the new eastern structure to the center of the SMC and its large extent argues for an SMC origin, we must consider other possibilities. Could this be a stream of the LMC, a satellite of the SMC, or something else entirely (e.g., MW halo substructure)? The new structure is likely not related to the LMC because the RC color is too blue. The LMC is more metal-rich ( $[Fe/H]\sim -0.4$ ) than the SMC ( $[Fe/H]\sim -1.0$ ; Pagel & Tautvaisiene 1998) and this difference would be evident in the mean RC color, which is metallicity-dependent (Girardi et al. 1998). For a 3.2 Gyr population ( $\log(\text{age})=9.5$ ), the Padova isochrones (Girardi et al. 2002) give a mean RC color of  $M-T_2\approx 1.05$  for  $[Fe/H]=-1.0$  and  $M-T_2\approx 1.22$  for  $[Fe/H]=-0.40$  with a difference of  $\sim 0.17$  mag. On the other hand, the observed mean RC colors in our MAPS LMC and SMC dereddened CMDs show a difference of  $\sim 0.04$ - $0.05$  mag, a smaller difference than from the theoretical isochrones, likely because we are sampling the more metal-poor peripheries of both objects. However, even a difference of  $\sim 0.05$  mag between the two components would be visible in the CMDs studied here. While there are some small changes in mean RC color with magnitude they are not more than  $\sim 0.01$ - $0.02$  mag (Fig. 3). Furthermore, for an LMC-origin, the density of the new structure should increase towards the LMC. However, we have two eastern fields at  $R=5.1^\circ$  from the SMC (closer to the LMC than the four eastern fields analyzed here) that have extended RCs but at *lower* densities than in the  $R=4.0^\circ$  fields (Fig. 11). This indicates that the new structure decreases in density from the SMC center, but not from the LMC center. The new structure is, therefore, unlikely to be related to the LMC.

The large extent in position angle of this structure (corresponding to  $\sim 9$  kpc), and its fairly uniform density across that distance, makes it unlikely to be a completely new satellite galaxy. A stream of a satellite galaxy of the SMC could span such a large region of the sky, but the density of the stream would have to rival that of

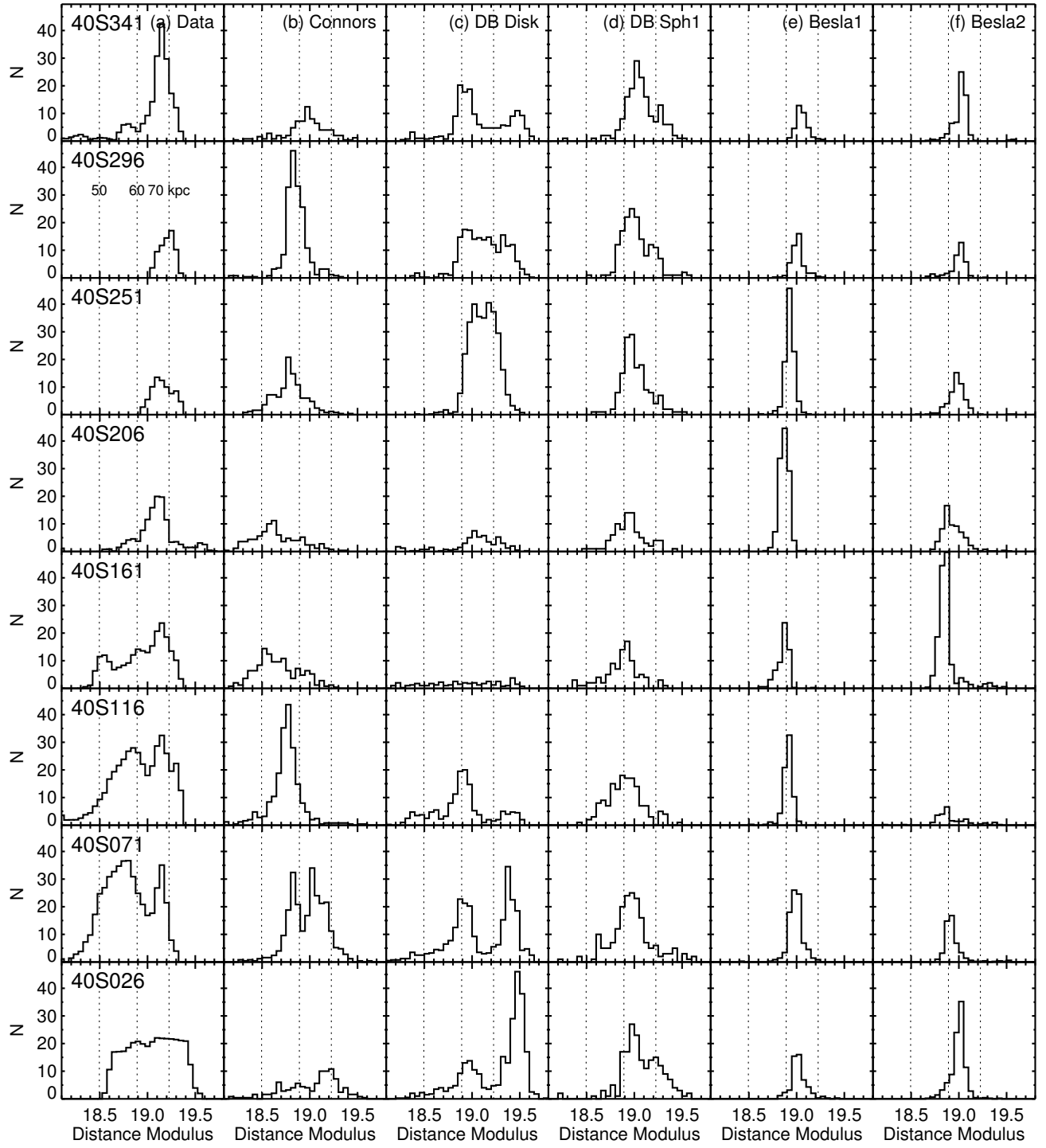


FIG. 9.— Density function with distance modulus for our red clump data and various models: (a) data, (b) Connors et al. (2006) model (scaled by 1/2.5), (c) Diaz & Bekki (2012) model disk component (scaled by 1/4), (d) Diaz & Bekki (2012) model spheroid1 component, (e) Besla et al. (2012) model1 (scaled by 1/3.5), and (f) Besla et al. (2012) model2 (scaled by 1/5). The field names are given in the upper left hand corner of column *a*. Vertical dotted lines indicate 50, 60 and 70 kpc.

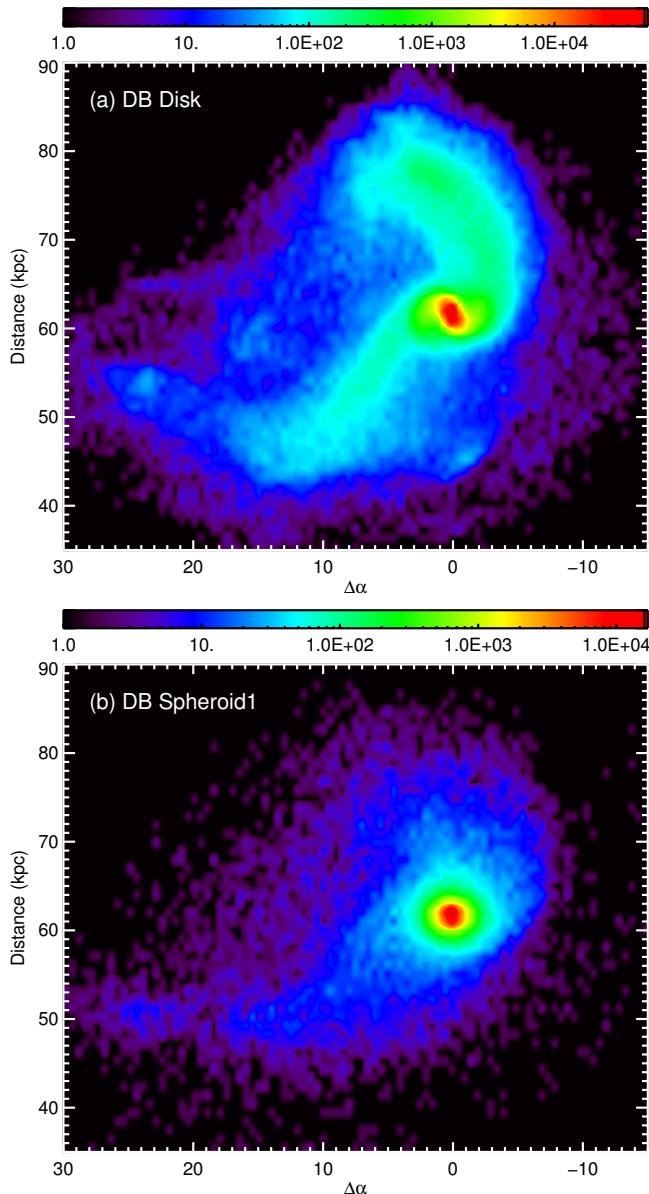


FIG. 10.— Distance- $\Delta\alpha$  diagrams for the Diaz & Bekki (2012) disk (a) and spheroid1 (b) models (for particles with  $|\Delta\delta| < 10^\circ$ ). Both models show the bridge extending to the east and closer distances, while only the disk model shows the counter-bridge prominently extending to distances of  $\sim 80$  kpc.

the SMC itself in those regions (and exceed it in some places), which would imply a truly massive satellite and a core that should have been previously detected.

A new MW halo substructure is also unlikely because it would need to have nearly the identical metallicity, position in the sky, and distance (closer by  $\sim 10$  kpc) as the SMC (producing a nearly identical distribution in the CMD) and, additionally, have a density fall-off with SMC radius. Therefore, we conclude that the most likely explanation is that the new component at  $d \sim 55$  kpc is a stream of the SMC itself. The new component’s location (to the east) and distance roughly match that expected for a tidally stripped stream of stars from the Diaz & Bekki (2012) simulations that were “loosened” in the last close encounter of the MCs  $\sim 200$  Myr ago.

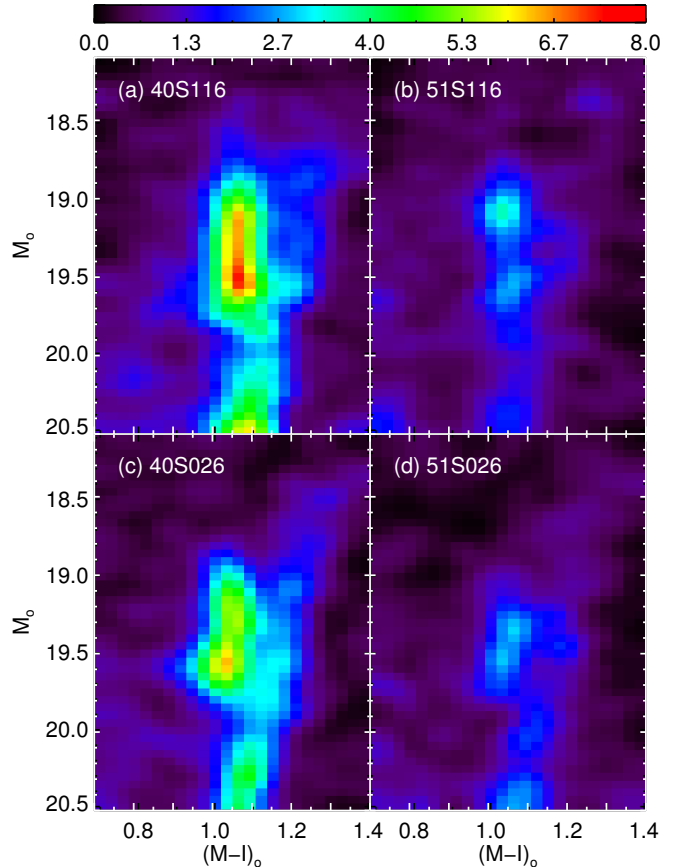


FIG. 11.— Hess diagrams showing the dependence of the density of the two distance components (at  $\sim 55$  kpc and  $\sim 67$  kpc) with SMC radius for two position angles. (a) 40S116, (b) 51S116, (c) 40S026, and (d) 51S026. At  $\text{PA}=116^\circ$  the density of both components drops with radius but the distant component more quickly than the closer component. At  $\text{PA}=26^\circ$  the density of both components again drops with radius but this time the closer component drops more rapidly (almost vanishing) than the distant component.

While it is more difficult to use RC stars to study the depth of the inner SMC (where there are many young stars) because of age effects, nevertheless such an extended RC as seen in the eastern SMC might be detectable. The RC luminosity function in the inner SMC ( $R \lesssim 2^\circ$ ), using MCPS (Zaritsky et al. 2002) and OGLE-III (Udalski et al. 2008) data, looks much more like those in our western fields than our eastern fields, and there is little variation in the shape of the RC with position angle and radius. However, there are three reasons why we are not likely to detect much structure in the density function with distance near the center of the SMC: (1) Near the center the density is very centrally-peaked (in distance) making it difficult to detect a lower-density structure at a non-systemic distance; at larger radii the density distribution is much less centrally-peaked and it becomes easier to detect deviations. (2) It is more difficult to strip stars from the center (because they are more tightly bound) than from the periphery. (3) For stripped stars, deviations in distance from the systemic value should grow with radius (see Fig. 10). Therefore, it is not too surprising that the RC shape in the central region of the SMC looks quite regular and any deviations become visible only at larger radius. We note that the

central SMC RR Lyrae also show little spatial pattern or variations and have a depth of only  $\sim 8$  kpc, similar to what we observe in our western fields (Haschke et al. 2012).

In the near future several wide-field photometric surveys will be able to provide the data needed to study the 3D structure of the SMC periphery in great detail. OGLE-IV (Kozłowski et al. 2013) will provide high-quality time-series photometry with which RR Lyrae and Cepheids can be identified and accurate distances measured, as was done by Haschke et al. (2012) with OGLE-III. OGLE-IV, SkyMapper (Keller et al. 2012) and DES (Abbott et al. 2012), as well as other DECam programs, will provide photometry to well-below the SMC horizontal branch over a large area of the MCs and with which RC stars can be exploited to study the 3D structure of the SMC.

We plan to study the radial velocities and metallicities of stars in the SMC periphery, especially in the east, to help understand any kinematical or chemical differences that may exist between the two components (as previously seen by Hatzidimitriou et al. 1993) and that might shed new light on the origin of the newly found stellar structure.

Finally, we note that the existence of a stellar structure *in front* of the main SMC stellar population could have important implications for microlensing surveys, in that this will increase the self-lensing of SMC stars (Besla et al. 2013; Calchi Novati et al. 2013). We recommend that this newly identified structure be taken into account in the analysis of microlensing surveys probing the eastern periphery of the SMC (e.g., OGLE-IV).

## 7. SUMMARY

We use high-quality CTIO-4m+MOSAIC photometry in eight fields at  $R=4^\circ$  in the SMC to study the outer galaxy’s line-of-sight distribution. Many of the fields show very extended red clump luminosity distributions, as previously seen by Hatzidimitriou & Hawkins (1989) and Gardiner & Hawkins (1991). We show that the extended red clump luminosity distributions cannot be accounted for by age effects because the main-sequence counterparts of very young populations ( $\lesssim 1$  Gyr) are not observed. Our main results and conclusions are:

1. The four eastern fields show very large line-of-sight depths ( $\sim 23$  kpc) over  $\sim 135^\circ$  of position angle.
2. Three eastern fields show a strong distance bimodality with one component at  $\sim 67$  kpc (near the

mean SMC distance) and a second component at  $\sim 55$  kpc. The fourth eastern field (40S026) has a broadened distance distribution, and is potentially consistent with the trend seen in the other three eastern fields but at slightly larger distances.

3. The newly-found stellar component in the east at  $\sim 55$  kpc is qualitatively consistent with the Diaz & Bekki (2012) model distribution of particles in the tidally-stripped Magellanic Bridge, previously only detected in HI. We conclude that this new component is likely an intermediate-age/old ( $\sim 1$ -12 Gyr) stellar component of the Magellanic Bridge and call it the SMC “eastern stellar structure”.

A tidally-stripped stellar component of the Magellanic Bridge is consistent with the discovery of accreted SMC stars in the LMC by Olsen et al. (2011) and the claim by Besla et al. (2013) of a tidal origin for the microlensing events reported towards the LMC. In the future, we plan to follow-up our discovery using spectroscopy in SMC fields to compare the stellar velocities to those predicted by the models for the Magellanic Bridge.

We find that even though there are some similarities between our data presented here and models from the literature, the differences are much more apparent and it is clear that more work is needed on the simulations to match the SMC stellar distribution. It might be that the stellar components of the SMC (disk or halo) are initially more extended than the simulations have so far considered.

We dedicate this paper to Robert T. Rood who did pioneering work on horizontal branch stars and found the extended SMC RC very fascinating. We thank J.D. Diaz, Gurtina Besla and Mario Mateo for useful discussions, and Diaz, Besla and Connors for sharing their models with us so we could compare them to our data. We also thank Sebastian Hidalgo for running IAC-star population synthesis models for us. We thank the OGLE and MCPS projects for making their SMC photometric databases available to the public, and Despina Hatzidimitriou for providing us with her photographic plate photometric of the SMC periphery. D.L.N. was supported by a Dean B. McLaughlin fellowship at the University of Michigan. E.F.B. acknowledges support from NSF grant AST 1008342. We acknowledge funding from NSF grants AST-0307851 and AST-0807945, and NASA/JPL contract 1228235. R.R.M. acknowledges support from CONICYT through project BASAL PFB-06 and from the FONDECYT project N°1120013.

*Facilities:* CTIO (MOSAIC II).

## REFERENCES

- Abbott, T., Abdalla, F., Achitouv, I., et al. 2012, *The Astronomer’s Telegram*, 4668, 1
- Aparicio, A., & Gallart, C. 2004, *AJ*, 128, 1465
- Bagheri, G., Cioni, M.-R. L., & Napiwotzki, R. 2013, *A&A*, 551, A78
- Beaulieu, J.-P., & Sackett, P. D. 1998, *AJ*, 116, 209
- Bekki, K., & Chiba, M. 2009, *PASA*, 26, 48
- Besla, G., Kallivayalil, N., Hernquist, L., Robertson, B., Cox, T. J., van der Marel, R. P., & Alcock, C. 2007, *ApJ*, 668, 949
- Besla, G., Kallivayalil, N., Hernquist, L., et al. 2010, *ApJ*, 721, L97
- Besla, G., Kallivayalil, N., Hernquist, L., et al. 2012, *MNRAS*, 421, 2109 (B12)
- Besla, G., Hernquist, L., & Loeb, A. 2013, *MNRAS*, 428, 2342
- Brüns, C., et al. 2005, *A&A*, 432, 45B (B05)
- Calchi Novati, S., Mirzoyan, S., Jetzer, P., & Scarpetta, G. 2013, *MNRAS*, 2104
- Caldwell, J. A. R., & Coulson, I. M. 1986, *MNRAS*, 218, 223
- Connors, T. W., Kawata, D., & Gibson, B. K. 2006, *MNRAS*, 371, 108
- Crowl, H. H., Sarajedini, A., Piatti, A. E., et al. 2001, *AJ*, 122, 220

- De Propris, R., Rich, R. M., Mallery, R. C., & Howard, C. D. 2010, *ApJ*, 714, L249
- Diaz, J. D., & Bekki, K. 2012, *ApJ*, 750, 36 (DB12)
- Gallart, C. 1998, *ApJ*, 495, L43
- Gardiner, L. T., & Hawkins, M. R. S. 1991, *MNRAS*, 251, 174
- Gardiner, L. T., & Hatzidimitriou, D. 1992, *MNRAS*, 257, 195
- Gardiner, L. T., & Noguchi, M. 1996, *MNRAS*, 278, 191
- Girardi, L., Groenewegen, M. A. T., Weiss, A., & Salaris, M. 1998, *MNRAS*, 301, 149
- Girardi, L., Bressan, A., Bertelli, G., & Chiosi, C. 2000, *A&AS*, 141, 371
- Girardi, L., Bertelli, G., Bressan, A., Chiosi, C., Groenewegen, M. A. T., Marigo, P., Salasnich, B., & Weiss, A. 2002, *A&A*, 391, 195
- Harris, J., & Zaritsky, D. 2006, *AJ*, 131, 2514
- Haschke, R., Grebel, E. K., & Duffau, S. 2012, *AJ*, 144, 107
- Hatzidimitriou, D., Hawkins, M. R. S., & Gyldenkerne, K. 1989, *MNRAS*, 241, 645
- Hatzidimitriou, D., & Hawkins, M. R. S. 1989, *MNRAS*, 241, 667
- Hatzidimitriou, D., Cannon, R. D., & Hawkins, M. R. S. 1993, *MNRAS*, 261, 873
- Keller, S. C., Skymapper Team, & Aegis Team 2012, *Galactic Archaeology: Near-Field Cosmology and the Formation of the Milky Way*, 458, 409
- Kozłowski, S., Udalski, A., Wyrzykowski, L., et al. 2013, *Acta Astron.*, 63, 1
- Kroupa, P. 2002, *Science*, 295, 82
- Kunkel, W. E., Demers, S., & Irwin, M. J. 2000, *AJ*, 119, 2789
- Majewski, S. R., Ostheimer, J. C., Kunkel, W. E., & Patterson, R. J. 2000, *AJ*, 120, 2550
- Mathewson, D. S., Ford, V. L., & Visvanathan, N. 1986, *ApJ*, 301, 664
- Mathewson, D. S., Ford, V. L., & Visvanathan, N. 1988, *ApJ*, 333, 617
- Muller, E., Staveley-Smith, L., Zealey, W., & Stanimirović, S. 2003, *MNRAS*, 339, 105
- Muller, E., & Bekki, K. 2007, *MNRAS*, 381, L11
- Murai, T., & Fujimoto, M. 1980, *PASJ*, 32, 581
- Nidever, D. L., Majewski, S. R., Butler Burton, W., & Nigra, L. 2010, *ApJ*, 723, 1618
- Nidever, D. L., Majewski, S. R., Muñoz, R. R., Beaton, R. L., Patterson, R. J., & Kunkel, W. E. 2011, *ApJ*, 733, L10
- Noël, N. E. D., & Gallart, C. 2007, *ApJ*, 665, L23
- Noël, N. E. D., Conn, B. C., Carrera, R., et al. 2013, *ApJ*, 768, 109
- Olsen, K. A. G., Zaritsky, D., Blum, R. D., Boyer, M. L., & Gordon, K. D. 2011, *ApJ*, 737, 29
- Pagel, B. E. J., & Tautvaisiene, G. 1998, *MNRAS*, 299, 535
- Pietrinferni, A., Cassisi, S., Salaris, M., & Castelli, F. 2004, *ApJ*, 612, 168
- Růžička, A., Theis, C., & Palouš, J. 2010, *ApJ*, 725, 369
- Schlegel, D. J., Finkbeiner, D. P., & Davis, M. 1998, *ApJ*, 500, 525
- Skrutskie, M. F., Cutri, R. M., Stiening, R., et al. 2006, *AJ*, 131, 1163
- Stanimirović, S., Staveley-Smith, L., & Jones, P. A. 2004, *ApJ*, 604, 176
- Sweigart, A. V. 1987, *ApJS*, 65, 95
- Udalski, A., et al. 2008, *Acta Astronomica*, 58, 329
- Xu, H. Y., & Li, Y. 2004, *A&A*, 418, 225
- Zaritsky, D., & Lin, D. N. C. 1997, *AJ*, 114, 2545
- Zaritsky, D., Harris, J., Grebel, E. K., & Thompson, I. B. 2000, *ApJ*, 534, L53
- Zaritsky, D., Harris, J., Thompson, I. B., Grebel, E. K., & Massey, P. 2002, *AJ*, 123, 855